AFRL-AFOSR-VA-TR-2020-0021

Seedling project on the simulation of reactive material particle combustion in high-explosive environments

Ryan Houim
UNIVERSITY OF FLORIDA

10/29/2019
Final Report

Air Force Research Laboratory
AF Office Of Scientific Research (AFOSR)/ RTA1
Arlington, Virginia 22203
Air Force Materiel Command

DISTRIBUTION A: Distribution approved for public release

REPORT DOCUMENTATION PAGE

Form Approved
OMB No. 0704-0188

1. REPORT DATE *(DD-MM-YYYY)*	2. REPORT TYPE	3. DATES COVERED *(From - To)*
17-03-2020	Final Performance	01 Aug 2018 to 31 Jul 2019

4. TITLE AND SUBTITLE
Seedling project on the simulation of reactive material particle combustion in high-explosive environments

5a. CONTRACT NUMBER

5b. GRANT NUMBER
FA9550-18-1-0389

5c. PROGRAM ELEMENT NUMBER
61102F

6. AUTHOR(S)
Ryan Houim

5d. PROJECT NUMBER

5e. TASK NUMBER

5f. WORK UNIT NUMBER

7. PERFORMING ORGANIZATION NAME(S) AND ADDRESS(ES)
UNIVERSITY OF FLORIDA
207 GRINTER HALL
GAINESVILLE, FL 32611-5500 US

8. PERFORMING ORGANIZATION REPORT NUMBER

9. SPONSORING/MONITORING AGENCY NAME(S) AND ADDRESS(ES)
AF Office of Scientific Research
875 N. Randolph St. Room 3112
Arlington, VA 22203

10. SPONSOR/MONITOR'S ACRONYM(S)
AFRL/AFOSR RTA1

11. SPONSOR/MONITOR'S REPORT NUMBER(S)
AFRL-AFOSR-VA-TR-2020-0021

12. DISTRIBUTION/AVAILABILITY STATEMENT
A DISTRIBUTION UNLIMITED: PB Public Release

13. SUPPLEMENTARY NOTES

14. ABSTRACT
This work implemented non-ideal equation of state, afterburning, and metal particle combustion models into the HyBurn code. The methods are demonstrated for a canonical problem of a high-explosive charge surrounded by an annular shell of aluminum particles. The results of the methods implemented by the HyBurn show the formation of particle fingers and the ignition and turbulent combustion of the dispersed Al particle cloud.

15. SUBJECT TERMS
reactive material, energetic materials, combustion models, afterburning

16. SECURITY CLASSIFICATION OF:			17. LIMITATION OF ABSTRACT	18. NUMBER OF PAGES	19a. NAME OF RESPONSIBLE PERSON
a. REPORT	b. ABSTRACT	c. THIS PAGE			SCHMIDT, MARTIN
Unclassified	Unclassified	Unclassified	UU		19b. TELEPHONE NUMBER *(Include area code)* 703-588-8436

Standard Form 298 (Rev. 8/98)
Prescribed by ANSI Std. Z39.18

Final Report

Seedling project on the simulation of reactive material particle combustion in high-explosive environments

AFOSR FA9550-18-1-0389

Program Participants:
PI: Dr. Ryan Houim
Mr. Swagnik Guhathakurta
Ms. Hsiao-Chi Li

University of Florida Department of Mechanical and Aerospace Engineering

Submitted to:
Air Force Office of Scientific Research (AFOSR)
AFSOR Technical Contact: Dr. Martin Schmidt

Period of Performance:
August 1, 2018 – July 31, 2019

Contents

1 Background and Introduction

1.1 Introduction

Reactive particles (RP) are being investigated for use in energetic systems due to their high specific energy density, long-duration energy release, and resultant increased explosive yields over traditional energetic materials that have high explosives (HE) as the main energetic component. Experimental tests have demonstrated that RP-enhanced devices can be highly effective. However, it is also known that the energetic yield from RP can vary tremendously depending on the subtle details the device and test environment. This is due to the complex interaction of physical, thermal, and chemical processes involved in reactive particle combustion, which are not well understood at present.

The aim of this seedling effort was to implement simulations tools and models into the HyBurn code (discussed below) that can be used to simulate the dispersal and combustion of RP by HE charges. In addition, the additions to the HyBurn code that were implemented in this project will ultimately lead to increased predictive modeling capabilities and improved physical understanding of RP-enhanced explosives. In addition, these additional capabilities have allowed for follow-up research programs that are aimed at understanding the fundamental physical processes of multiphase blasts.

1.2 Overview of The HyBurn Code

HyBurn is a unique Eulerian multiphase reactive flow code that is robust and is capable of simulating the extreme conditions associated with RP-enhanced explosives as demonstrated in this project. HyBurn is highly efficient and scalable by its use of the AMReX [1] block-structured adaptive mesh refinement (AMR) library [1]. In addition, HyBurn has been ported to several DoD high-performance computing systems.

HyBurn uses state-of-the-art Eulerian multiphase and granular compaction models [2] and has been used to study the coal mine explosions [3; 4], the interaction between dense particle beds and shock waves [5], and the explosive dispersal of comet regolith [6]. The numerical solution techniques used by HyBurn are based on a high-order Godunov algorithm [2; 7]. These algorithms are robust enough to simulate dust explosions [3; 4], deflagration-to-detonation transition [8], and shock-to-detonation transition [9].

A complete listing of the governing equations solved by HyBurn for particulate multiphase flows is given in Appendix A.

1.3 Project Tasks

The particle combustion and equation-of-state (EOS) models that were implemented in HyBurn were appropriate for studying coal mine and other organic dust explosions for safety applications. Prior to this project, the models implemented in HyBurn were not applicable for simulating RP-enhanced explosives. The primary objective of this work was to add appropriate EOS and energetic particle (Al) models to HyBurn and demonstrate its use as a robust tool for simulating reactive particle-laden blasts. To achieve that, a major effort of

this one-year seedling project was be to implement existing EOS and particle afterburning models into HyBurn that are appropriate for HE environments.

This project was divided into three technical tasks. A brief summary of the tasks and their results are discussed below. Section 2 describes details of the results from these tasks.

1.3.1 Task 1: Implement metal particle combustion models into HyBurn

The objective of this task was to implement a model for reactive particle combustion, which was focused on aluminum for this work. The Al particle cloud afterburning model of Kuhl *et al.* [10; 11] was selected based on an ongoing collaboration with Dr. Allen Kuhl (LLNL) and its applicability to explosive environments.

1.3.2 Task 2: Implement a non-ideal equations of state into HyBurn

The objective of this task was to implement a non-ideal equation of state model into HyBurn to more accurately compute the thermodynamic state observed by the reactive particles and the initial shock wave. In addition, this task also implemented afterburning models for fuel-rich HE detonation products.

1.3.3 Task 3: Demonstrate the capabilities of the extended HyBurn code

The goal of this task was to demonstrate the capabilities and robustness of the extended HyBurn code for simulating enhanced blast scenarios with afterburning of fuel-rich high-explosive detonation products and aluminum particles. This demonstration problem was designed to illustrate the extended capabilities of HyBurn developed in Tasks 1 and 2 and, additionally, to serve as the beginning steps for follow-up research programs and collaborations with AFRL/RW.

2 Results and Summary of Accomplishments

The results of the three technical tasks are discussed here. Each of these tasks has successively increased the capabilities of HyBurn to simulate multiphase blasts with significant afterburning.

In this section we focus on the models that have been added to HyBurn and some of the implementation details. The full set of equations solved by HyBurn for a generic multiphase reactive flow are given in Appendix A.

2.1 Task 1: Implement metallic particle combustion models into HyBurn

A literature survey was performed on metal particle combustion models that were developed for use in detonation and explosive environments [10–12]. Ultimately, the model of Kuhl *et al.* [10; 11] was selected because it has been demonstrated for use in high-explosive environments. This particular model was also selected because it requires data only on the particle burning and ignition delay times, which makes it extensible to other reactive material particles under consideration by the Air Force.

The Al particle combustion model of Kuhl *et al.* [10; 11] follows an ignition-delay model where the ignition and combustion progresses occur in two separate steps. The first step calculates the ignition of the particles. The second step burns the particles after they have ignited.

2.1.1 Al Ignition

An ignition variable, f, is constructed to track a dimensionless ignition delay time of the particles [10]

$$\frac{\partial \alpha_s \rho_s f}{\partial t} + \boldsymbol{\nabla}\cdot\alpha_s\rho_s\mathbf{v}_s f = \frac{\alpha_s\rho_s}{\tau_{ign}(T, Y_i)}, \tag{1}$$

where τ_{ign} is the experimentally determined ignition delay time of the particle, T is the local gas-phase temperature, and Y_i represents the local gas-phase mass fraction of species i. If $f \geq 1$ the particles are considered to be ignited and then burn provided that the particle temperature, T_s is greater than the ignition temperature, T_{ign}.

The ignition delay time is fit to experimental measurements using an Arrhenius model [10]

$$\tau_{ign} = \frac{1}{A}\exp\left(-\frac{T_a}{T}\right), \tag{2}$$

where the pre-exponential factor A and activation temperature T_a are constants to be determined. For spherical aluminum particles of diameter 6 μm, $A = 4 \times 10^{10}$ s and $T_a = 30,000$ K [10].

Data indicate that the activation temperature has a relatively small dependence on the particle diameter for the Al particle diameters of interest for this project (between 2 and 50 μm). The pre-exponential factor for particles of different diameters are corrected based on

ignition delay time correlations,

$$A = A_0 \left(\frac{d_0}{d} \right)^{2.3}, \tag{3}$$

where $A_0 = 4 \times 10^{10}$ s and $d_0 = 6$ μm.

The ignition temperature, T_{ign}, of Al is given by [10]

$$T_{ign} = T_{melt} - \left[0.6 + \frac{C_{ox}^{0.3} d_s}{\lambda} e^{-0.85\sqrt{ds}} \right], \tag{4}$$

where C_{ox} is the effective oxidizer concentration [13; 14], d_s is the initial particle diameter, and $T_{melt} = 2300$ is the melting point of the protective oxide layer surrounding the Al core.

2.1.2 Al Combustion

After ignition, $f \geq 1$ and $T_s > T_{ign}$, the particles are allowed to burn with the surrounding oxidizer. (T_s is the particle temperature.) The global reaction for Al burning with air (on a mass basis) is

$$\mathrm{Al} + \nu_{\mathrm{Al}} \mathrm{Air} \longrightarrow (1 + \nu_{\mathrm{Al}}) \mathrm{Prod}_{\mathrm{Al}}, \tag{5}$$

where ν_{Al} is the mass Air-fuel ratio for Al combustion, $\nu_{Al} = 4.03$. The products of Al combustion are modeled as a lumped gas-phase species and include nitrogen, aluminum oxide, aluminum sub-oxides, etc. [10].

The mass exchange rate of Al per unit volume used as the phase change source term in the governing equations, $\dot{m}'''_{Al}$, is [10; 12]

$$\dot{m}'''_{Al} = 3\alpha_s \rho_{Al} \frac{1 + 0.276\sqrt{Re_d}}{t_{burn}}, \tag{6}$$

where t_{burn} is the empirical Al particle burning time, $\rho_A l$ is the density of solid aluminum (2700 kg m^{-3}), and the Reynolds number is

$$Re_d = \frac{\rho_g d_s |\boldsymbol{v}_g - \boldsymbol{v}_s|}{\mu_g}, \tag{7}$$

where ρ_g is the local gas density, $\boldsymbol{v}_g$ is the gas-phase velocity vector, mu_g is the gas-phase viscosity, and $\boldsymbol{v}_s$ is the particle velocity.

The burning time can be given from an empirical D^n correlation or directly from experimental data [14–16]. Here we use a traditional D^2 correlation [10]

$$t_{burn} = K d_s^2, \tag{8}$$

where $K = 1.5 \times 10^6$ s/m^2 for air.

The correlation of Lynch *et al.* [14] will be used in future studies to account for Al particle combustion in oxidizing mixtures such as H_2O and CO_2 and to capture the change of the diameter exponent, n, when the Al particles transition from a diffusion-limited combustion regime to a chemical-kinetic limited regime [15; 16].

2.1.3 Implementation of Particle Burning in HyBurn

HyBurn uses an operator splitting approach to solve the governing equations where the hydrodnamic and particle advection terms are solved separately from the inhomogenous source terms arising from particle drag, combustion, phase change, etc. [2; 7; 17; 18]. For example, the equation for the ignition delay variable , f, is solved in two-steps. The first step transports f for a time step of Δt by updating

$$\frac{\partial \alpha_s \rho_s f}{\partial t} + \boldsymbol{\nabla} \cdot \alpha_s \rho_s \mathbf{v}_s f = 0. \tag{9}$$

This equation is fully coupled with all of the other gas- and granular-phase transport equations.

Next, the local source terms are integrated. For f, this means solving

$$\frac{d\alpha_s \rho_s f}{dt} = \frac{\alpha_s \rho_s}{\tau_{ign}(T, Y_i)} \tag{10}$$

at each grid point. The ignition delay variable is integrated in isolation from all other reactions. This simplification makes the granular bulk density ($\alpha_s \rho_s$) and T_g constant during chemical integration of f. As a result, the local ignition delay time is constant during integration and f can be updated simply by

$$f = f^0 + \frac{\Delta t}{\tau_{ign}} = f^0 + \Delta t A e^{-\frac{T_a}{T_g}}, \tag{11}$$

where f^0 is the initial condition.

After ignition ($f \geq 1$ and $T \geq T_{ign}$) the aluminum burns, which produces the following three linearly dependent differential equations that describes the consumption of Al, consumption of air, and production of Al-air combustion products

$$\frac{d\alpha_s \rho_{Al}}{dt} = -\dot{m}'''_{Al} = -3\alpha_s \rho_{Al} \frac{1 + 0.276\sqrt{Re_d}}{t_{burn}}, \tag{12}$$

$$\frac{d\alpha_g \rho_g Y_{Air}}{dt} = -\nu_{Al} \dot{m}'''_{Al}, \tag{13}$$

$$\frac{d\alpha_g \rho_g Y_{Prod_{Al}}}{dt} = (1 + \nu_{Al})\, \dot{m}'''_{Al}. \tag{14}$$

Similar to f, these reactive particle burning equations are integrated in isolation from the other source terms. This forces the particle Reynolds number and burning time to be constant during the chemical integration. The aluminum that is consumed δM is assumed to instantly react with the available oxidizer. Thus, the total particle mass consumed is limited either by the amount of available air or the aluminum mass consumed by the analytical integration of Eqn. (12), which ever is smaller

$$\delta M = \min \left[\alpha_s \rho_{Al} \left(1 - e^{C\Delta t}\right), \frac{\alpha_g \rho_g Y_{g,Air}}{\nu_{Al}} \right], \tag{15}$$

where

$$C = 3\frac{1 + 0.276\sqrt{Re_d}}{t_{burn}}. \tag{16}$$

Finally the updated masses of the Al particles, air, and aluminum-air products is

$$\begin{aligned} \alpha_s \rho_{Al} &= (\alpha_s \rho_{Al})^0 - \delta M \\ \alpha_g \rho_g Y_{Air} &= (\alpha_g \rho_g Y_{Air})^0 - \nu_{Al} \delta M \\ \alpha_g \rho_g Y_{Prod_{Al}} &= (\alpha_g \rho_g Y_{Prod_{Al}})^0 + (1 + \nu_{Al})\, \delta M \end{aligned} \tag{17}$$

2.2 Task 2: Non-Ideal Equation of State and Gas-Phase Afterburning

Here we present the non-ideal equation of state and afterburning model that has been implemented into HyBurn. The non-ideal equation of state is a modified JWL model that accounts for multicomponent gas-phase mixtures, non-constant specific heats, and the enthalpy of formation for each species [10].

2.2.1 JWL Model for Mixtures

The pressure for the gas-phase is given by a modified JWL equation of state

$$p = A \left[1 - \frac{\omega \rho_g}{R_1 \rho_0}\right] \exp\left(-R_1 \frac{\rho_0}{\rho_g}\right) + B \left[1 - \frac{\omega \rho_g}{R_2 \rho_0}\right] \exp\left(-R_2 \frac{\rho_0}{\rho_g}\right) + \rho_g R_{mix} T_g, \tag{18}$$

where A, B, R_1, R_2, ω, and ρ_0 are ρ_g is the gas-phase density, T_g is the gas-phase temperature, and

$$R_{mix} = Ru \sum \frac{Y_{g,i}}{Mw_i}, \tag{19}$$

Ru is the universal gas constant, $Y_{g,i}$ is the mass fraction of gas-phase species i, and Mw_i is the molecular weight of gas-phase species i. In this formulation, the mixture JWL model is a thermally perfect equation of state for a mixture of ideal gases with a non-linear barotropic correction factor.

2.2.2 Internal Energy

The gas-phase mixture internal energy, e_g, is

$$e_g(T_g, Y_{g,i}) = \sum Y_{g,i} e_i(T_g), \tag{20}$$

where e_i is the internal energy for species i. Following Kuhl *et al.* [10], the internal energy for each species is computed using piece-wise second-order polynomials, where

$$e_i(T) = a_{i,m} T_g^2 + b_{i,m} T_g + c_{i,m} \tag{21}$$

and m is an index that corresponds to the temperature interval of the polynomial. The parameter m is defined such that

$$m = j \quad \text{if} \quad T_j^B \leq T < T_{j+1}^B, \tag{22}$$

where T_j^B and T_{j+1}^B are the lower and upper temperature bounds of polynomial j, respectively.

The temperature is computed from the internal mixture energy using the positive root of second-order polynomials

$$T = \frac{-b_{mix} + \sqrt{b_{mix}^2 - 4a_{mix}\left(c_{mix} - e_g\right)}}{2a_{mix}}, \tag{23}$$

where

$$a_{mix} = \sum Y_i a_{i,m}, \quad b_{mix} = \sum Y_i b_{i,m}, \quad c_{mix} = \sum Y_i c_{i,m}. \tag{24}$$

When computing temperature from internal energy, the polynomial interval m is found based on the internal energy of the mixture based on the lower and upper temperature bounds of the polynomials. First, we define the internal energy of all species at the boundaries of each polynomial

$$e_{i,m}^B = e_i(T_m). \tag{25}$$

Then, when computing temperature from internal energy, the polynomial interval is computed from

$$m = j \quad \text{if} \quad \sum Y_i e_{i,j}^B \leq e < \sum Y_i e_{i,j+1}^B. \tag{26}$$

Note that this internal energy formulation neglects the nonlinear pressure from JWL. That is, the second term of the change in internal energy for a real gas,

$$de = CvdT - \left[P - T\left(\frac{\partial P}{\partial T}\right)_v\right] dv, \tag{27}$$

is neglected for the nonlinear JWL pressure. This should have a relatively small effect on the computations in this work. The neglected nonlinear energy is typically only important in the initial stages of the blast. However, the focus of these calculations is on the long duration dispersal and combustion of the reactive powder where the pressure is typically less than 10 atm. Our future work will examine efficient methods to include the nonlinear pressure contribution to the internal energy in order to quantitatively asses the modeling error introduced by this assumption.

2.2.3 Speed of Sound

The speed of sound, c is given by

$$c^2 = c_{\text{ideal}}^2 + c_{\text{JWL}}^2. \tag{28}$$

The ideal sound speed is

$$c_{\text{ideal}}^2 = \gamma R_{mix} T_g, \tag{29}$$

where

$$\gamma = \frac{Cv_{mix} + R_{mix}}{Cv_{mix}}, \tag{30}$$

and the mixture constant-volume specific heat is

$$Cv_{mix} = 2a_{mix}T_g + b_{mix}. \tag{31}$$

The non-ideal sound speed is

$$\begin{aligned} c_{JWL}^2 =& A\left[\left(R_1\frac{\rho_0}{\rho_g}-\omega\right)\frac{1}{\rho_g}-\frac{\omega}{R_1\rho_0}\right]\exp\left(-R_1\frac{\rho_0}{\rho_g}\right)+ \\ & B\left[\left(R_2\frac{\rho_0}{\rho_g}-\omega\right)\frac{1}{\rho_g}-\frac{\omega}{R_2\rho_0}\right]\exp\left(-R_2\frac{\rho_0}{\rho_g}\right) \end{aligned} \tag{32}$$

2.2.4 Gas-Phase Afterburning

The combustion of fuel-rich detonation products is assumed to be infinite rate (mixing-limited) and proceeds in a single-step irreversible reaction

$$\text{Fuel} + \nu_{\text{Fuel}}\text{Air} \longrightarrow (1+\nu_{\text{Al}})\text{Prod}_{\text{Fuel}}, \tag{33}$$

where ν_{Fuel} is the mass air-fuel ratio for the fuel (TNT detonation products for this work).

The gas-phase afterburning step in HyBurn is implemented as

$$\alpha_g\rho_g\frac{dY_i}{dt} = \alpha_g\dot{\omega}_i, \tag{34}$$

where $\dot{\omega}_i$ is the mass rate of production for species i. The afterburning reaction is assumed to progress infinitely fast. Thus, any fuel and air in a computational cell is burned instantly to produce products and left-over fuel or air. These infinite rate reactions are integrated by defining the change of product mass fraction based on the limiting reactant

$$\delta Y_P = \min\left[Y_{\text{Fuel}}^0\left(1+\nu_{\text{Fuel}}\right), Y_{\text{Air}}^0\frac{1+\nu_{\text{Fuel}}}{\nu_{\text{Fuel}}}\right]. \tag{35}$$

Then, the updated mass fractions are

$$Y_{\text{Fuel}} = Y_{\text{Fuel}}^0 - \delta Y_P\frac{1}{1+\nu_{\text{Fuel}}}, \tag{36}$$

$$Y_{\text{Air}} = Y_{\text{Air}}^0 - \delta Y_P\frac{\nu_{\text{Fuel}}}{1+\nu_{\text{Fuel}}}, \tag{37}$$

$$Y_{\text{Prod}} = Y_{\text{Prod}}^0 + \delta Y_P. \tag{38}$$

In the event that there is more than one fuel (such as multiple high-explosive materials), each reaction is updated independently in the order that they are listed in the input file. This allows HyBurn users to setup scenarios where reactions preferentially burn with an oxidizer without needing to use a finite-rate chemical-kinetic formulation.

2.3 Task 3: Demonstration Problem

The ignition and combustion of explosively-dispersed aluminum powder was selected as the demonstration problem using the extended HyBurn code. The physical setup and initial conditions are shown in Fig. 1. A spherical high-explosive (TNT) charge of radius 5 cm is surrounded by a 3-cm thick annular shell of aluminum particles. The diameter and volume fraction of the Al particles in the annular shell are 6 μm and 50%, respectively. The initial

conditions inside of the TNT charge are TNT-detonation products at 2870 K and 9.09 GPa (the constant-volume explosion limit). The gas outside of the TNT charge is air at 300 K and 1 atm.

The charge is detonated inside of a cylindrical chamber of radius 2 m and height 4 m. The simulations are performed in 2D axisymmetric coordinates (the x-axis is the radial direction) and half-symmetry is used in the y-direction. Adaptive mesh refinement is use with a minimum grid spacing of $\Delta x_{\min} = 1.95$ mm.

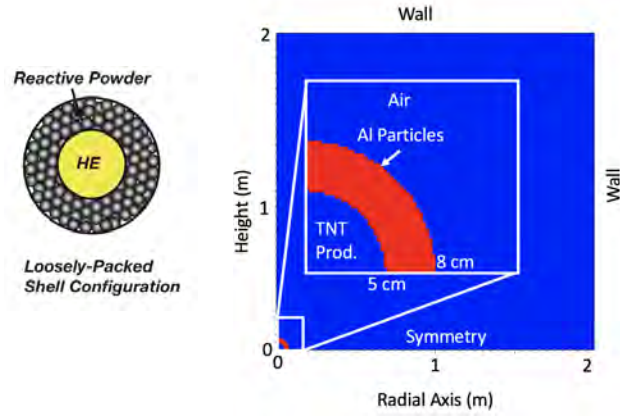

Figure 1: Schematic of (left) the high-explosive charge configuration and (right) the initial conditions of the demonstration simulation.

The simulation consists of 4 lumped species: TNT-detonation products, TNT-air combustion products, aluminum-air combustion products, and air. The internal energy of these lumped species are shown in Fig. 2. The molecular weights, reference properties, and internal energy polynomials are given in Appendix B.

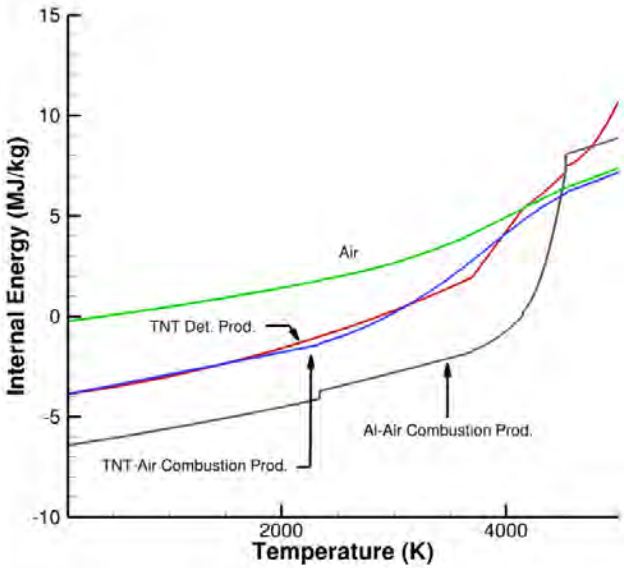

Figure 2: Internal energy for each gas-phase species as a function of temperature.

A time-sequence of the computed Al particle dispersal and combustion is shown in Fig. 3.

A detailed discussion of the physics is beyond the scope of this project, but is the subject of an ongoing AFOSR-funded Young Investigator Program. The results show the formation of Al particle fingers similar to those that have been observed in experiments [19]. The particles disperse to a much larger radius than the TNT fireball due their higher inertia. The simulation results at 1.58 and 2.57 ms show that the particle have completely separated from the TNT fireball. At later times the gas and particles start to contract and move towards the change center during the negative phase of the blast. The inertia of the particles carries them through to surface of the TNT fireball, which acts as an ignition source. The particles interact with the fireball and ignite at $\sim$4 ms. The particles continue to burn as a turbulent Al dust flame until they are consumed.

Figure 4 shows the overpressure and impulse measured at the location indicated in top-left image of Fig. 3. The burning Al particles clearly have a substantial effect on the overpressure and impulse. The quasi-static overpressure after the particles have almost completely burned is $\sim$ 3 bar. A similar simulation with no Al particles produced a quasi-static overpressure of only 0.8 bar.

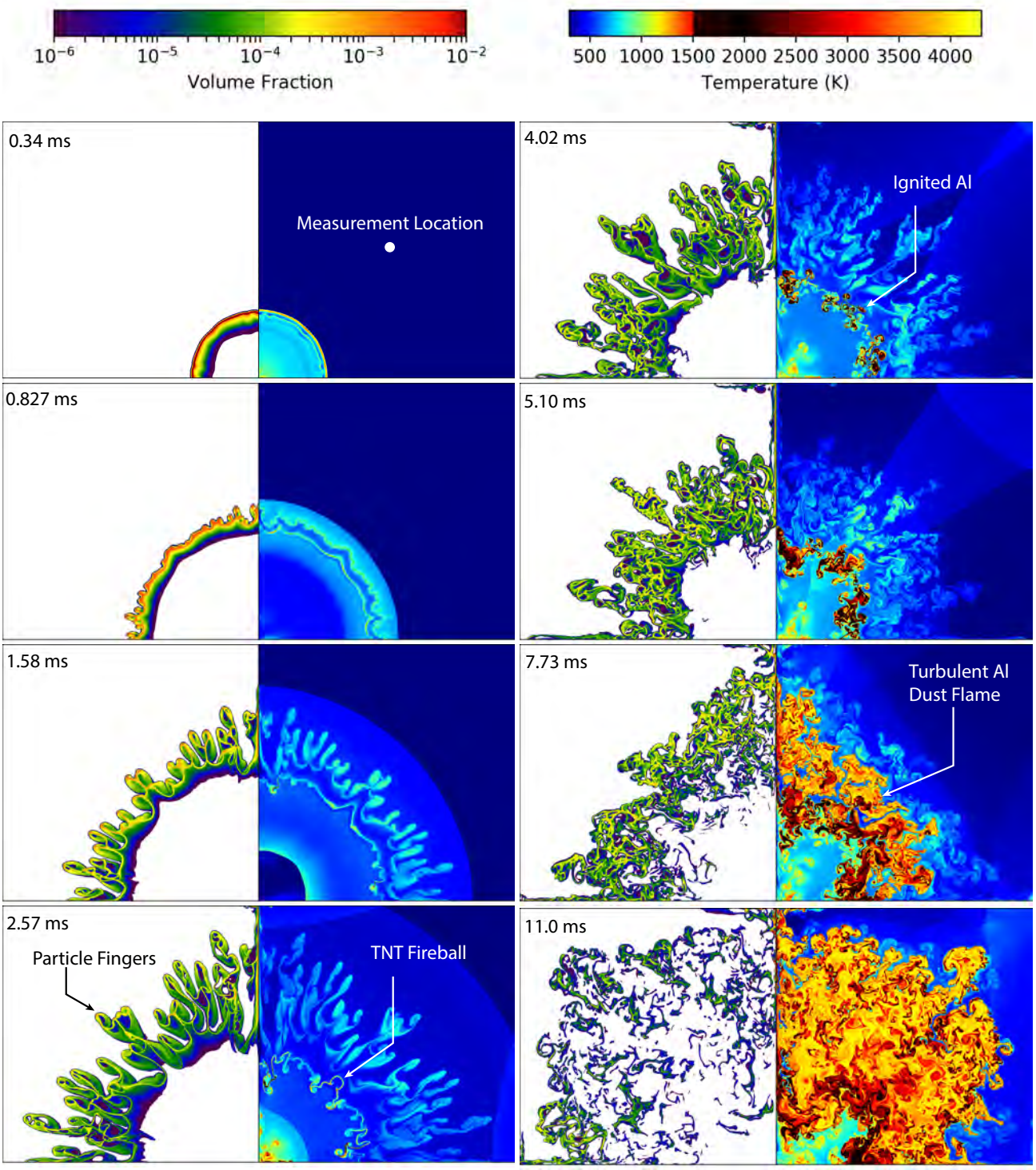

Figure 3: Time sequence of images showing the dispersal and combustion of the Al particles by a TNT charge. The left side of each image shows the Al particle volume fraction and right side shows the gas temperature.

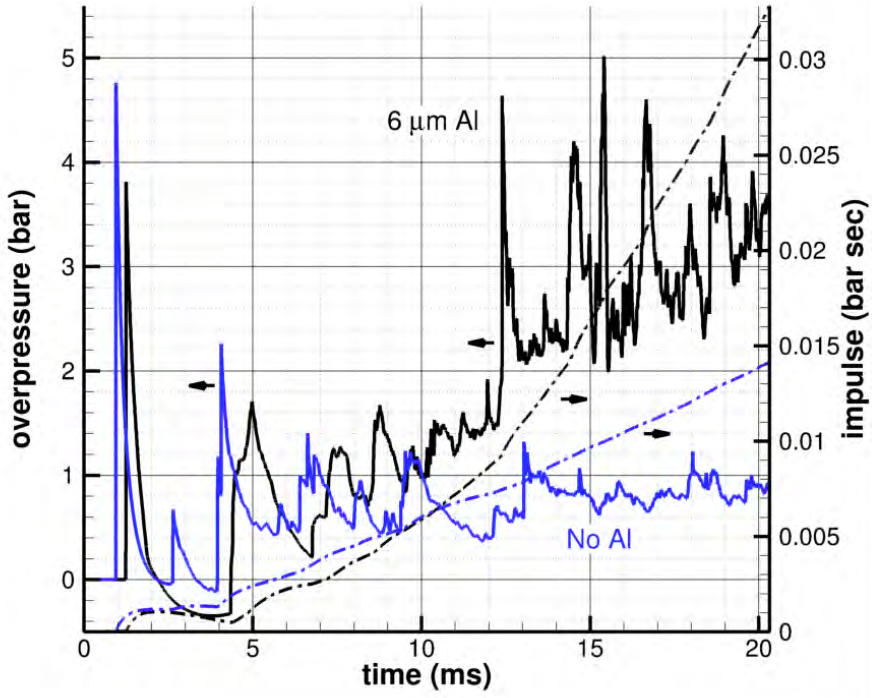

Figure 4: The computed overpressure and impulse measured the center of the domain, as indicated in Fig. 3.

3 Transition to the Air Force and Department of Energy

The HyBurn code, with the capabilities added throughout this project, have been made available to AFRL/RW and is being used by Drs. Brian Taylor and Matthew Clay for some of their lab work.

The HyBurn code is also being considered for use by Drs. Allen Kuhl, David Grote, and Jens Von Der Linden of LLNL to simulate a variety of phenomena ranging from particle laden blasts to supersonic particulate-laden jet flow during the eruption of a volcano.

4 Publications and Presentations

The publications and presentations based on the work performed in this project are listed here.

4.1 Publications that are in Preparation

1. Houim, R. W., Guhathakurta, S., Taylor, B., Kuhl, A., "Ignition and Combustion of Explosively Dispersed Aluminum Particles," *Proceedings of the Combustion Institute*, In Preparation.

4.2 Conference Presentations

1. Houim, R. W., "Numerical Simulation of Explosively-Dispersed Reactive Poweder," American Physical Society Topical Group on Shock Compression of Condensed Matter, Portland, Oregon, June 16-21, 2019 (Presented by Dr. Brian Taylor of AFRL/RW)

4.3 Invited Seminars

1. Houim, R. W., "Details on Coupling a Compressible Gas to Dense Granular Media, Lawrence Berkely National Laboratory", Berkeley, California, Jan 8, 2019

2. Houim, R. W., "Application of Granular Physics to High Speed Reactive Flow", Lawrence Livermore National Laboratory, Livermore, California, Jan 9, 2019

3. Houim, R. W., "Dispersal and Combustion of Reactive Powder by Shock Waves," University of Central Florida, Orlando, Florida, Jan 18, 2019

A Equations Solved by HyBurn

Here we present the governing equations solved by HyBurn. Additional details can be found in [2].

A.1 Gas-Phase Equations

The gas-phase equations in HyBurn are the Navier-Stokes equations that have been modified to include the presence of granular particles. The volume taken up by the particles is included through the gas-phase volume fraction α_g [20],

$$\frac{\partial \alpha_g \rho_g}{\partial t} + \boldsymbol{\nabla}\boldsymbol{\cdot}(\alpha_g \rho_g \boldsymbol{v}_g) = S^M \tag{39}$$

$$\frac{\partial \alpha_g \rho_g Y_{g,j}}{\partial t} + \boldsymbol{\nabla}\boldsymbol{\cdot}[\alpha_g \rho_g Y_{g,j} \left(\boldsymbol{v}_g + \boldsymbol{V}_{g,i}\right)] = \alpha_g \dot{\boldsymbol{\omega}}_{g,j} + S^Y_{g,j}; \quad j = 1, \cdots, N_g \tag{40}$$

$$\frac{\partial \alpha_g \rho_g \boldsymbol{v}_g}{\partial t} + \boldsymbol{\nabla}\boldsymbol{\cdot}(\alpha_g \rho_g \boldsymbol{v}_g \boldsymbol{v}_g) + \alpha_g \boldsymbol{\nabla} p_g = \alpha_g \rho_g \boldsymbol{g} + \boldsymbol{\nabla}\boldsymbol{\cdot}\left(\alpha_g \tau_g\right) + \boldsymbol{S^p} \tag{41}$$

$$\frac{\partial \alpha_g \rho_g E_g}{\partial t} + \boldsymbol{\nabla}\boldsymbol{\cdot}[\alpha_g \boldsymbol{v}_g (\rho_g E_g + p_g)] = -p_g \, \boldsymbol{\nabla}\boldsymbol{\cdot}\left(\alpha_s \boldsymbol{v}_s\right) \tag{42}$$

$$+ \boldsymbol{\nabla}\boldsymbol{\cdot}\left(\alpha_g \boldsymbol{q}\right) + \boldsymbol{\nabla}\boldsymbol{\cdot}\left(\alpha_g \boldsymbol{v_g} \cdot \tau_g\right) + \alpha_g \rho_g \boldsymbol{g} \boldsymbol{\cdot} \boldsymbol{v}_g + S^E_g \tag{43}$$

where the subscript g refers to the gas and s refers to the particles and α_s and α_g are the volume fraction of particles and gas, respectively. The volume fractions have the property

$$\alpha_g + \alpha_s = 1 \quad \text{and} \quad \boldsymbol{\nabla}\alpha_g = -\boldsymbol{\nabla}\alpha_s, \tag{44}$$

The quantities $Y_{g,j}$, ρ_g, p_g, T_g, E_g, $\boldsymbol{v}_g$, τ_g, and $\boldsymbol{q}$, are the volume fraction, mass fraction of species j, density, pressure, temperature, total energy, velocity vector, deviatoric stress tensor, and diffusive heat flux vector of the gas, respectively. The reaction rate due to homogeneous chemical reactions is denoted by $\dot{\boldsymbol{\omega}}_{g,j}$. Additional interphase coupling terms describing transfer of mass, momentum and energy between the gas and the particles are denoted by S^M, $S^Y_{g,j}$, $\boldsymbol{S^p}$, S^E_g. Several of these are described in section A.3.

A.2 Particle-Phase Equations

The governing equations for the particles essentially a set of Euler equations that are not unlike that of a gas [21]. The primary difference is that compressibility of the granular phase is introduced by changes in solid volume fraction rather than the material density of the particles. Here, the material density of the solid particles is assumed to be constant.

The granular-phase governing equations for mass, momentum, pseudo-thermal energy (random translational kinetic energy of the particles needed to represent collisions), and internal energy with N_s species within each particle are:

$$\frac{\partial \alpha_s \rho_s}{\partial t} + \boldsymbol{\nabla}\boldsymbol{\cdot}(\alpha_s \rho_s \boldsymbol{v}_s) = -S^M \tag{45}$$

$$\frac{\partial \alpha_s \rho_s Y_{s,j}}{\partial t} + \boldsymbol{\nabla}\cdot(\alpha_s \rho_s Y_{s,j} \boldsymbol{v}_s) = \alpha_s \dot{\boldsymbol{\omega}}_{s,j} + S^Y_{s,j}; \quad j = 1, \cdots, N_s \tag{46}$$

$$\frac{\partial \alpha_s \rho_s \boldsymbol{v}_s}{\partial t} + \boldsymbol{\nabla}\cdot(\alpha_s \rho_s \boldsymbol{v}_s \boldsymbol{v}_s) + \boldsymbol{\nabla} p_s + \boldsymbol{\nabla} p_{\text{fric}} = -\alpha_s \boldsymbol{\nabla} p_g + \alpha_s \rho_s \boldsymbol{g} - \boldsymbol{S^p} \tag{47}$$

$$\frac{\partial \alpha_s \rho_s E_s}{\partial t} + \boldsymbol{\nabla}\cdot(\alpha_s \rho_s E_s \boldsymbol{v}_s) = -p_s \boldsymbol{\nabla}\cdot \boldsymbol{v}_s + S^{\text{PTE}}_s \tag{48}$$

$$\frac{\partial \alpha_s \rho_s e_s}{\partial t} + \boldsymbol{\nabla}\cdot(\alpha_s \rho_s e_s \boldsymbol{v}_s) = S^E_s, \tag{49}$$

where p_s, p_{fric}, e_s, E_s, and $\dot{\gamma}$ are the solids pressure derived from kinetic theory, friction-collisional pressure, internal energy, pseudo-thermal energy, and dissipation of E_s due to inelastic particle collisions, respectively. The homogeneous reaction rate of granular species i is denoted by $\dot{\omega}_{s,i}$. The additional interphase coupling terms, $S^Y_{s,j}$, S^{PTE}_s, and S^E_s, are discussed in section A.3.

The pseudo-thermal energy (PTE), E_s, represents the energy due to random translational motion of the particles,

$$E_s = \frac{3}{2}\Theta_s. \tag{50}$$

It is a function of the granular temperature, Θ_s, defined as the mean-square of the particle velocity fluctuations [21–23].

The thermodynamic temperature of the particles, T_s, is computed from the solid sensible internal energy, e_s, through

$$e_s = \sum_{j=1}^{N_s} Y_{s,j} \left(e^0_{fj} + \int_{T_0}^{T_s} C_{V,s,j}(s) ds \right), \tag{51}$$

where N_s is the number of species in the solid phase, e^0_{fj} is an internal energy of formation, and $C_{V,s,j}$ is the constant-volume specific heat of species j in the particle phase.

The solids pressure, p_s, represents collisional effects of the particles and is given by an equation of state for a granular gas [21],

$$p_s = \alpha_s \rho_s \Theta_s [1 + 2(1+e)\alpha_s g_0], \tag{52}$$

where e is the coefficient of restitution. The radial distribution function, g_0, is defined by [21],

$$\frac{1}{g_0} = 1 - \left(\frac{\alpha_s}{\alpha_{s,\max}} \right)^{1/3}, \tag{53}$$

where $\alpha_{s,\max}$ is the packing limit, which is an input parameter that we set to 0.65.

When particles occupy a high volume fraction, frictional-collisional pressure, p_{fric} must be added to p_s to describe pressure-like forces of particle grains that in constant contact

$$p_{\text{fric}} = \begin{cases} 0 & \text{if } \alpha_s < \alpha_{s,\text{crit}} \\ 0.1\alpha_s \dfrac{(\alpha_s - \alpha_{s,\text{crit}})^2}{(\alpha_{s,\max} - \alpha_s)^5} & \text{if } \alpha_s \geq \alpha_{s,\text{crit}}, \end{cases} \tag{54}$$

where $\alpha_{s,\text{crit}}$ is 0.5.

A.3 Interphase Coupling Terms

Source terms that couple the governing equations for the gas and granular phases include drag, convective heat transfer, phase change, and dissipation of PTE from inelastic collisions, and lifting forces.

The mass exchange term due to phase change is

$$S^M = \dot{m}'''. \tag{55}$$

The momentum source terms resulting from phase change, drag, and lift are

$$\boldsymbol{S^p} = \boldsymbol{f}_{\text{Drag}} + \boldsymbol{f}_{\text{Lift}} + \boldsymbol{v}_{\text{int}}\dot{M}. \tag{56}$$

The drag force for the particulate mixture is given by the correlation of **(author?)** [21]

$$\boldsymbol{f}_{\text{drag}} = K_{sg}(\boldsymbol{v}_s - \boldsymbol{v}_g), \tag{57}$$

where

$$K_{sg} = \begin{cases} 0.75 C_d \dfrac{\rho_g \alpha_g \alpha_s |\boldsymbol{v}_s - \boldsymbol{v}_g|}{d_s \alpha_g^{2.65}} & \text{if } \alpha_g \geq 0.8 \\ 150 \dfrac{\alpha_s^2 \mu_g}{\alpha_g d_s^2} + 1.75 \dfrac{\rho_g \alpha_s |\boldsymbol{v}_g - \boldsymbol{v}_s|}{d_s} & \text{if } \alpha_g < 0.8, \end{cases} \tag{58}$$

the drag coefficient, C_d, is

$$C_d = \begin{cases} 24(\alpha_g Re)^{-1}[1 + 0.15(\alpha_g Re)^{0.687}] & \text{if } \alpha_g Re < 1000 \\ 0.44 & \text{if } \alpha_g Re \geq 1000, \end{cases} \tag{59}$$

and the Reynolds number is defined by

$$Re = \frac{\rho_g |\boldsymbol{v}_g - \boldsymbol{v}_s| d_s}{\mu_g}. \tag{60}$$

The lift force, $\boldsymbol{f}_{\text{Lift}}$, is modeled using the Magnus lift force defined by

$$\boldsymbol{f}_{\text{Lift}} = C_l \alpha_s \rho_g (\boldsymbol{v}_s - \boldsymbol{v}_g) \times (\boldsymbol{\nabla} \times \boldsymbol{v}_g), \tag{61}$$

where the lift coefficient, C_l, has a value of 0.5 [24].

The interfacial velocity used for momentum exchange and energy during phase change are defined using the value from the phase that is loosing mass,

$$\boldsymbol{v}_{\text{int}} = \begin{cases} \boldsymbol{v}_s & \text{if } \dot{m}''' > 0 \\ \boldsymbol{v}_g & \text{if } \dot{m}''' < 0. \end{cases} \tag{62}$$

The source terms in the energy equations are

$$S_g^{\text{E}} = -q_{\text{conv}} + \phi_{\text{visc}} + E_{g,\text{int}}\dot{m}''' + (\boldsymbol{f}_{\text{Drag}} + \boldsymbol{f}_{\text{Lift}}) \cdot \boldsymbol{v}_s, \tag{63}$$

$$S_s^{\text{E}} = q_{\text{conv}} - e_{s,\text{int}}\dot{m}''' + \dot{\gamma}, \tag{64}$$

$$S_s^{\text{PTE}} = -\dot{\gamma} - \phi_{\text{visc}} - E_{s,\text{int}}\dot{m}''', \tag{65}$$

where $E_{g,\text{int}} = H_{g,\text{int}} - p_{\text{int}}/\rho_s$. These energy exchange term include, in addition to convective heat transfer, effects from dissipation of PTE from inelastic particle collisions ($\dot{\gamma}$) and dissipation of PTE due to viscous effects (ϕ_{visc}).

The convective heat flux between the gas and particles is

$$q_{\text{conv}} = 6\frac{\alpha_s \lambda_g Nu}{d_s^2}(T_g - T_s), \tag{66}$$

where the Nusselt number is estimated using correlation of [25]

$$Nu = (7 - 10\alpha_g + 5\alpha_g^2)(1 + 0.7Re^{0.2}Pr_g^{1/3}) + (1.33 - 2.4\alpha_g + 1.2\alpha_g^2)Re^{0.7}Pr_g^{1/3} \tag{67}$$

and Pr_g is the gas-phase Prandtl number.

The model for viscous damping of PTE is adopted from [21]

$$\phi_{\text{visc}} = 3K_{sg}\Theta_s. \tag{68}$$

The rate of internal energy production into the gas phase due to frictional heating during particle drag is

$$q_{\text{drag}} = \Delta\boldsymbol{v} \cdot \boldsymbol{f}_{\text{Net}}, \tag{69}$$

where $\boldsymbol{f}_{\text{Net}} = \boldsymbol{f}_{\text{Drag}} + \boldsymbol{f}_{\text{Lift}}$ and $\Delta\boldsymbol{v} = \boldsymbol{v}_s - \boldsymbol{v}_g$.

The granular dissipation model adopted for this study [26] is a variant of Haff's cooling law [23; 27],

$$\dot{\gamma} = \frac{12(1-e^2)g_0\alpha_s^2}{\sqrt{\pi}}\frac{\rho_s\Theta_s^{3/2}}{d_s}. \tag{70}$$

Similar to the $\boldsymbol{v}_{\text{int}}$, the interfacial energy exchange terms for phase change are defined by the phase that is loosing mass

$$E_{g,\text{int}} = \begin{cases} e_s + E_s + \boldsymbol{v}_s \cdot \boldsymbol{v}_s /2 & \text{if } \dot{m}''' > 0 \\ E_g & \text{if } \dot{m}''' < 0, \end{cases} \quad E_{s,\text{int}} = \begin{cases} E_s & \text{if } \dot{m}''' > 0 \\ 0 & \text{if } \dot{m}''' < 0, \end{cases} \tag{71}$$

$$e_{s,\text{int}} = \begin{cases} e_s & \text{if } \dot{m}''' > 0 \\ E_g - \boldsymbol{v}_g \cdot \boldsymbol{v}_g /2 & \text{if } \dot{m}''' < 0. \end{cases} \tag{72}$$

B Species Thermodynamic Properties

Four gas-phase species were considered in this work: TNT-products, TNT-air combustion products, air, and Al-air combustion products. Their thermodynamic input parameters are presented below.

The thermodynamic data involve five temperature intervals that are listed below These

Table 1: Boundaries temperatures for the polynomials.

m	1	2	3	4	5	6
T	300	2340	3700	4150	4530	6000

polynomials are formed based on fits to the Cheetah chemical equilibrium code [10] where the internal energy for each lumped species is computed assuming chemical equilibrium if the temperature is greater than 1800 K.

The viscosity is computed using

$$\mu = \mu_0 \sqrt{\frac{T}{273}} \tag{73}$$

and the thermal conductivity is computed using

$$\lambda = \lambda_0 \sqrt{\frac{T}{273}} \tag{74}$$

A simple mole-fraction weighted mixing rule is used to compute the mixture thermal conductivity and viscosity

$$\begin{aligned} \mu_{mix} &= \sum X_i \mu_i \\ \lambda_{mix} &= \sum X_i \lambda_i \end{aligned} \tag{75}$$

B.1 TNT Detonation Products

The Molecular weight is: $MW = 26.9$ kg/kmol

The afterburning reaction proceeds as

$$\mathrm{TNT_{Prod}} + \nu_{\mathrm{TNT}} \mathrm{Air} \longrightarrow (1 + \nu_{\mathrm{Al}}) \mathrm{TNT\_Air_{Prod}},$$

where $\nu_{TNT} = 3.35$

The reference transport properties are

$$\begin{aligned} \lambda_0 &= 0.02096 \text{ W/mK} \\ \mu_0 &= 1.245 \times 10^{-5} \text{ Pa s} \end{aligned}$$

The polynomial coefficients are:

Table 2: Polynomial coefficients for TNT detonation products in units of cal/g.

m	a	b	c
1	5.3244e-5	0.17393	-941.33
2	7.9903e-5	0.035886	-760.12
3	0.0000	1.80555	-6211.8
4	4.5108e-4	-2.7713	5014.0
5	2.578e-3	-22.917	52697.0

B.2 TNT-Air Combustion Products

The Molecular weight is: $MW = 26.65$ kg/kmol

The reference transport properties are

$$\lambda_0 = 0.0186 \text{ W/mK}$$
$$\mu_0 = 1.53 \times 10^{-5} \text{ Pa s}$$

The polynomial coefficients are:

Table 3: Polynomial coefficients for TNT-air combustion products in units of cal/g.

m	a	b	c
1	3.5282e-6	0.25361	-949.3
2	2.5302e-4	-0.80169	168.08
3	-6.1238e-5	1.5345	-4178
4	-3.9217e-4	4.2413	-9713.6
5	2.7654e-5	0.2432	-195.0

B.3 Air

The Molecular weight is: $MW = 28.85$ kg/kmol

The reference transport properties are

$$\lambda_0 = 0.024 \text{ W/mK}$$
$$\mu_0 = 1.716 \times 10^{-5} \text{ Pa s}$$

The polynomial coefficients are:

B.4 Aluminum-Air Combustion Products

The Molecular weight is: $MW = 40.78$ kg/kmol

The reference transport properties are

$$\lambda_0 = 0.024 \text{ W/mK}$$
$$\mu_0 = 1.716 \times 10^{-5} \text{ Pa s}$$

The polynomial coefficients are:

Table 4: Polynomial coefficients for air in units of cal/g.

m	a	b	c
1	2.02768e-5	0.16498	-71.9172
2	1.34322e-4	-0.41045	658.24424
3	7.01281e-5	0.11507	-403.36139
4	-1.02084e-4	1.53731	-3340.674
5	4.04923e-5	0.11381	148.38643

Table 5: Polynomial coefficients for aluminum-air combustion products in units of cal/g.

m	a	b	c
1	1.49115e-5	0.2502	-1554.5182
2	1.49115e-5	0.2502	-1554.5182
3	0.00113	-7.95255	13553.8
4	0.00826	-67.29752	137084.51
5	5.03544e-5	-0.07059	1216.0279

C Aluminum Particle Properties

The material density of the particles is $\rho_{Al} = 2700$ kg/m^3.

The internal energy is computed by:

$$e_{Al} = e_{ref} + Cv_{Al}T,$$

where $e_{ref} = -35,101$ J/kg and $Cv_{Al} = 1177$ J/kg K.

The global reaction for Al burning with air is

$$\mathrm{Al} + \nu_{\mathrm{Al}}\mathrm{Air} \longrightarrow (1 + \nu_{\mathrm{Al}})\mathrm{Prod}_{\mathrm{Al}}, \tag{76}$$

where $\nu_{Al} = 4.03$.

References

[1] Zhang, W., Almgren, A., Beckner, V., Bell, J., Blaschke, J., Chan, C., Day, M., Friesen, B., Gott, K., Graves, D., Katz, M., P., Myers, A., Nguyen, T., Nonaka, A., Rosso, M., Williams, S., and Zingale, M., "AMReX: a framework for block-structured adaptive mesh refinement," *Journal of Open Source Software*, Vol. 4, 2019, pp. 1370.

[2] Houim, R. W. and Oran, E. S., "A Multiphase Model for Compressible Granular-Gaseous Flows: Formulation and Initial Tests," *Journal of Fluid Mechanics*, Vol. 789, 2016, pp. 166–220.

[3] Houim, R. W. and Oran, E. S., "Numerical simulation of dilute and dense layered coal-dust explosions," *Proceedings of the Combustion Institute*, Vol. 35, No. 2, 2015, pp. 2083 – 2090.

[4] Houim, R. W. and Oran, E. S., "Structure and flame speed of dilute and dense layered coal-dust explosions," *Journal of Loss Prevention in the Process Industries*, Vol. 36, 2015, pp. 214–222.

[5] Ugarte, O. J., Houim, R. W., and Oran, E. S., "Examination of the forces controlling dust dispersion by shock waves," *Physical Review Fluids*, Vol. 2, 2017, pp. 074304.

[6] Lai, S., Houim, R. W., and Oran, E. S., "Mechanism and structure of subsurface explosions in granular media," *Phys. Rev. Fluids*, Vol. 2, Sep 2017, pp. 094301.

[7] Houim, R. W. and Kuo, K. K., "A low-dissipation and time-accurate method for compressible multi-component flow with variable specific heat ratios," *Journal of Computational Physics*, Vol. 230, No. 23, 2011, pp. 8527–8553.

[8] Houim, R. W., Ozgen, A., and Oran, E. S., "The role of spontaneous waves in the deflagration-to-detonation transition in submillimetre channels," *Combustion Theory and Modelling*, Vol. 20, No. 6, 2016, pp. 1068–1087.

[9] Houim, R. W. and Taylor, B. D., "Detonation initiation from shock and material interface interactions in hydrogen-air mixtures," *Proceedings of the Combustion Institute*, Vol. 37, No. 3, 2019, pp. 3513 – 3520.

[10] Kuhl, A., Bell, J., and Beckner, V., "Heterogeneous Continuum Model of Aluminum Particle Combustion in Explosions," *Combustion, Explosion, and Shock Waves*, Vol. 46, No. 4, 2010, pp. 433–448.

[11] Kuhl, A. L., Bell, J. B., Beckner, V. E., Balakrishnan, K., and Aspden, A. J., "Spherical combustion clouds in explosions," *Shock Waves*, Vol. 23, No. 3, May 2013, pp. 233–249.

[12] Benkiewicz, K. and Hayashi, A., "Aluminum dust ignition behind reflected shock wave: two-dimensional simulations," *Fluid Dynamics Research*, Vol. 30, No. 5, 2002, pp. 269–292.

[13] Beckstead, M., "Correlating Aluminum Burning Times," *Combustion, Explosion, and Shock Waves*, Vol. 41, 2005, pp. 533–546, 10.1007/s10573-005-0067-2.

[14] Lynch, P., Krier, H., and Glumac, N., "A correlation for burn time of aluminum particles in the transition regime," *Proceedings of the Combustion Institute*, Vol. 32, No. 2, 2009, pp. 1887–1893.

[15] Bazyn, T., Krier, H., and Glumac, N., "Oxidizer and Pressure Effects on the Combustion of 10-μm Aluminum Particles," *Journal of Propulsion and Power*, Vol. 21, No. 4, 2005, pp. 577–582.

[16] Bazyn, T., Krier, H., and Glumac, N., "Combustion of Nanoaluminum at Elevated Pressure and Temperature Behind Reflected Shock Waves," *Combustion and Flame*, Vol. 145, 2006, pp. 703–713.

[17] Toro, E. F., *Riemann Solvers and Numerical Methods for Fluid Dynamics*, Springer, New York, NY, 2nd ed., 1999.

[18] Oran, E. S. and Boris, J. P., *Numerical Simulation of Reactive Flow*, Cambridge, New York, NY, 2nd ed., 2001.

[19] Frost, D. L., Gregoire, Y., Patel, O., Goroshin, S., and Zhang, F., "Particle jet formation during explosive dispersal of solid particles," *Physics of Fluids*, Vol. 24, 2012, pp. 091109.

[20] Ishii, M. and Hibiki, T., *Thermo-Fluid Dynamics of Two-Phase Flow*, Springer, New York, 2006.

[21] Gidaspow, D., *Multiphase Flow and Fluidization*, Academic Press, 1994.

[22] Van Wachem, B. G. M., Schouten, J. C., van den Bleek, C. M., Krishna, R., and Sinclair, J. L., "Comparative analysis of CFD models of dense gas–solid systems," *AIChE Journal*, Vol. 47, No. 5, 2001, pp. 1035–1051.

[23] Brilliantov, N. V. and Pöschel, T., *Kinetic Theory of Granular Gases*, Oxford University Press, 2004.

[24] Drew, D. and Lahey Jr., R., "The virtual mass and lift force on a sphere in rotating and straining inviscid flow," *International Journal of Multiphase Flow*, Vol. 13, No. 1, 1987, pp. 113 – 121.

[25] Gunn, D. J., "Transfer of Heat of Mass to Particles in Fixed and Fluidized Beds," *Internatioal Journal of Heat and Mass Transfer*, Vol. 21, 1978, pp. 467–476.

[26] Lun, C., Savage, S., Jeffrey, D., and Chepurniy, N., "Kinetic theories for granular flow: inelastic particles in Couette flow and slightly inelastic particles in a general flowfield," *Journal of Fluid Mechanics*, Vol. 140, 1984, pp. 223–256.

[27] Haff, P., "Grain flow as a fluid-mechanical phenomena," *Journal of Fluid Mechanics*, Vol. 134, 1983, pp. 401–430.